AIP | Review of Scientific Instruments

A new endstation at the Swiss Light Source for ultraviolet photoelectron spectroscopy, X-ray photoelectron spectroscopy, and X-ray absorption spectroscopy measurements of liquid solutions

Matthew A. Brown, Amaia Beloqui Redondo, Inga Jordan, Nicolas Duyckaerts, Ming-Tao Lee et al.

Citation: Rev. Sci. Instrum. **84**, 073904 (2013); doi: 10.1063/1.4812786
View online: http://dx.doi.org/10.1063/1.4812786
View Table of Contents: http://rsi.aip.org/resource/1/RSINAK/v84/i7
Published by the AIP Publishing LLC.

A new endstation at the Swiss Light Source for ultraviolet photoelectron spectroscopy, X-ray photoelectron spectroscopy, and X-ray absorption spectroscopy measurements of liquid solutions

Matthew A. Brown,[1,a)] Amaia Beloqui Redondo,[1] Inga Jordan,[2] Nicolas Duyckaerts,[1] Ming-Tao Lee,[3] Markus Ammann,[3] Frithjof Nolting,[3] Armin Kleibert,[3] Thomas Huthwelker,[3] Jean-Pierre Mächler,[1] Mario Birrer,[3] Juri Honegger,[3] Reto Wetter,[3] Hans Jakob Wörner,[2] and Jeroen A. van Bokhoven[1,3,a)]

[1]*Institute for Chemical and Bioengineering, ETH Zürich, CH-8093 Zürich, Switzerland*
[2]*Laboratory of Physical Chemistry, ETH Zürich, CH-8093 Zürich, Switzerland*
[3]*Paul Scherrer Institute, CH-5232 Villigen PSI, Switzerland*

(Received 14 May 2013; accepted 18 June 2013; published online 12 July 2013)

A new liquid microjet endstation designed for ultraviolet (UPS) and X-ray (XPS) photoelectron, and partial electron yield X-ray absorption (XAS) spectroscopies at the Swiss Light Source is presented. The new endstation, which is based on a Scienta *HiPP-2* R4000 electron spectrometer, is the first liquid microjet endstation capable of operating in vacuum and in ambient pressures up to the equilibrium vapor pressure of liquid water at room temperature. In addition, the Scienta *HiPP-2* R4000 energy analyzer of this new endstation allows for XPS measurements up to 7000 eV electron kinetic energy that will enable electronic structure measurements of bulk solutions and buried interfaces from liquid microjet samples. The endstation is designed to operate at the soft X-ray SIM beamline and at the tender X-ray Phoenix beamline. The endstation can also be operated using a Scienta 5 K ultraviolet helium lamp for dedicated UPS measurements at the vapor-liquid interface using either He I or He II α lines. The design concept, first results from UPS, soft X-ray XPS, and partial electron yield XAS measurements, and an outlook to the potential of this endstation are presented. [http://dx.doi.org/10.1063/1.4812786]

I. INTRODUCTION

Electron spectroscopy from liquids has a long history that dates to the pioneering work of Siegbahn, *ESCA Applied to Liquids*, published in 1973.[1] In the 40 years since Siegbahn's first spectrum of liquid formamide, electron spectroscopy for chemical analysis (ESCA) from liquids has been revolutionized.[2–7] Three major advances have made this possible. Most important was the advent of third generation synchrotron radiation facilities, such as the Swiss Light Source[8] (SLS), that produce brilliant tunable X-ray beams that create a flux of photoelectrons from the liquid sample that dwarfs that produced by the conventional anode X-ray source used in the laboratory of Siegbahn. Modern day electron spectrometers have also helped.[9] They offer increased detection efficiency (transmission) and greatly improved resolution that not only increase the signal-to-noise ratio of a spectrum but can now also resolve near-overlapping electronic structures that in the past went undetected. Finally, the development of a vacuum liquid microjet[10–12] has allowed for studies of high vapor pressure liquids, such as neat water,[13,14] dilute electrolyte solutions,[15] and organic solutes[16] under ionization chamber pressures of ca. 10^{-4} mbar. Performing electron spectroscopy of liquids under vacuum eliminates a large fraction of the inelastic scattering the photoelectron experiences during ambient pressure liquid studies[17,18] while also reducing the gas phase contribution to the spectrum. Both have helped to reduce ambiguity in spectral assignments.

Using a liquid microjet as the sample delivery platform presents several advantages over studying the vapor-liquid interface of static samples.[2–7] The liquid microjet provides a continuously refreshed interface that remains free of the adventitious carbon impurities that plague static measurements at the vapor-liquid interface.[19] The continuously refreshed interface limits beam damage to the sample.[19,20] In addition, the liquid microjet makes virtually any liquid sample compatible with electron spectroscopy, which provides an endless array of opportunities for cross-collaboration between research fields and disciplines.[7]

We describe the development of a new endstation at the Swiss Light Source for *in situ* X-ray photoelectron (XP) and X-ray absorption (XA) spectroscopies of liquid solutions. The endstation can also be operated away from a synchrotron beamline with a helium (He) discharge lamp for ultraviolet photoelectron spectroscopy (UPS) studies of the vapor-liquid interface. The design of our apparatus is unique in several ways that help to distinguish it from the liquid jet endstations at BESSY[2] and MAX-lab.[21] The first is that it can be operated under a vacuum of ca. 10^{-4} mbar and in an ambient environment at background pressures up to 20 mbar. Designed as a mobile endstation adapted for both the SIM[22] and Phoenix beamlines of the Swiss Light Source, it allows for electron spectroscopy measurements from liquid solutions over an electron kinetic range that spans from 2 to 7000 eV.

a)Authors to whom correspondence should be addressed. Electronic addresses: matthew.brown@chem.ethz.ch and jeroen.vanbokhoven@chem.ethz.ch

Efficient photoelectron detection from liquid samples at low energies (ca. <60 eV) is a by-product of both a measurement chamber completely shielded of magnetic fields that can disrupt photoelectron trajectories at these energies, and the development of an electrostatic lens mode that applies a biased potential to the first lens element that helps to draw the low energy photoelectrons into the high vacuum environment of the electron analyzer where the mean free path is increased. This allows for electron spectroscopy measurements down to several eV and for use with a He discharge lamp for UPS measurements from the liquid microjet.

The remainder of the article is organized as follows: In Sec. II A, we describe the design of the liquid microjet endstation at the Swiss Light Source, in Sec. II B we present the accelerating lens mode of the electron analyzer that was developed specifically for liquid microjet studies at electron kinetic energies below 60 eV, and in Sec. II C the different entrance cones that can be used in the experiments. Section III describes the vacuum system. Section IV describes the motion control system designed to align the spectrometer to the beamline. In Secs. V A–V C, we present proof-of-principle results taken under vacuum using the liquid microjet at the soft X-ray SIM[22] beamline (XPS), using He II α excitation (UPS), and at the tender X-ray Phoenix beamline (partial electron yield XAS), respectively. Finally, we conclude in Sec. VI and provide an outlook of the potential of this new endstation.

II. THE LIQUID MICROJET ENDSTATION OF THE SWISS LIGHT SOURCE

A. Design concept

Figure 1(a) shows a picture of the liquid microjet endstation installed at the SIM[22] beamline of the Swiss Light Source. At the heart of the design is a Scienta *HiPP-2* R4000 electron spectrometer with a multi-channel plate (MCP) detector. The electron spectrometer is similar to that previously described,[9] and only features specifically relevant to the liquid microjet experiment are described here. The electron spectrometer is mounted parallel to the laboratory floor and has six electrostatic lens elements, three in the pre-lens and three in the (traditional) lens (Figure 1(b)). The analyzer is rotated on its side to align the entrance slits with the direction of flow of the liquid microjet. All the components of the liquid microjet are designed to operate inside a 6-way DN-200 aluminum cube that overlaps the orthogonal incoming photon beam, liquid microjet, and focal point of the electron spectrometer at its center (Figure 1(c)). The liquid microjet cube and all of its components were designed to be as compact as possible. Using a DN-200 cube improves access to the liquid microjet inside the chamber and greatly improves visibility/sight lines to the measurement area. To the top of the DN-200 cube is fitted a tee connector that houses a liquid nitrogen cold trap, used to condense water vapor and help to reduce the background chamber pressure, and a Agilent TwisTorr 700 turbo molecular pump. For experiments conducted in ambient pressures both the LN_2 trap and the turbo pump are removed and the flange blanked off with a viewport. The flange opposite the electron spectrometer is equipped with a pressure gauge, a viewport in direct line of sight up the electron spectrometer lens, and a linear/rotation feed-through manipulator that is used to seal off the entrance to the electron spectrometer during venting (discussed in Sec. II C). The incoming photon beam enters the DN-200 cube parallel to the floor. The opposite flange is used as a large viewport.

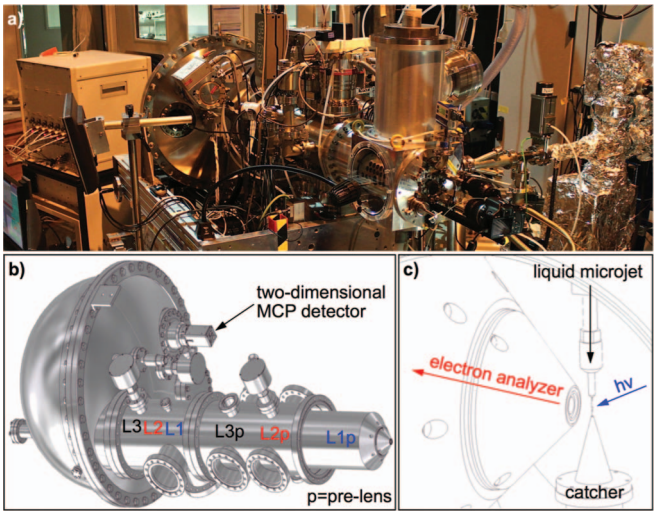

FIG. 1. (a) The liquid microjet endstation installed at the SIM beamline of the Swiss Light Source. (b) The Scienta *HiPP-2* R4000 electron spectrometer has six lens elements, three in the pre-lens and three in the (traditional) lens. (c) The incoming photon beam, the liquid microjet direction of flow, and the electron analyzer detection axis are orthogonal with one another.

The liquid microjet is mounted on the bottom DN-200 flange (Figure 2(a)). All materials are made of aluminum or titanium and are therefore free of magnetic fields. The liquid microjet consists of a titanium rod assembly and a quartz nozzle that has been described previously.[2] A three-axis piezo type in-vacuum motor with a step resolution of 100 nm controls the position of the liquid microjet. The motors are mounted directly to a rigid 12 mm thick motor mount that is attached to the DN-200 flange. The liquid microjet is expanded inside the vacuum chamber for ca. 1.5 cm (Figure 3) before it exits the chamber through a 600 μm hole in the aluminum catcher. The catcher is directly drained out the bottom of the measurement chamber and allows for the solution under investigation to be recycled. The remaining component mounted to the bottom flange is the spring-loaded bottom plate of the mu-metal shield that lines the DN-200 cube. A schematic representation of the mu-metal liner is shown in Figure 2(b). The field inside the chamber when the liquid microjet is mounted is less than 0.014 μT. In line with the simplicity of the overall setup, the mu-metal liner has been designed to allow simple access to the measurement area. The large side door can be quickly removed and provides a large enough access point to directly reach inside the chamber for minor adjustments.

B. Accelerating lens mode for low energy photoelectrons

It is difficult to develop a single electron spectrometer that is capable of detecting photoelectrons from the UV (ca. 2 eV) up to hard X-ray energies (7000 eV). Because our

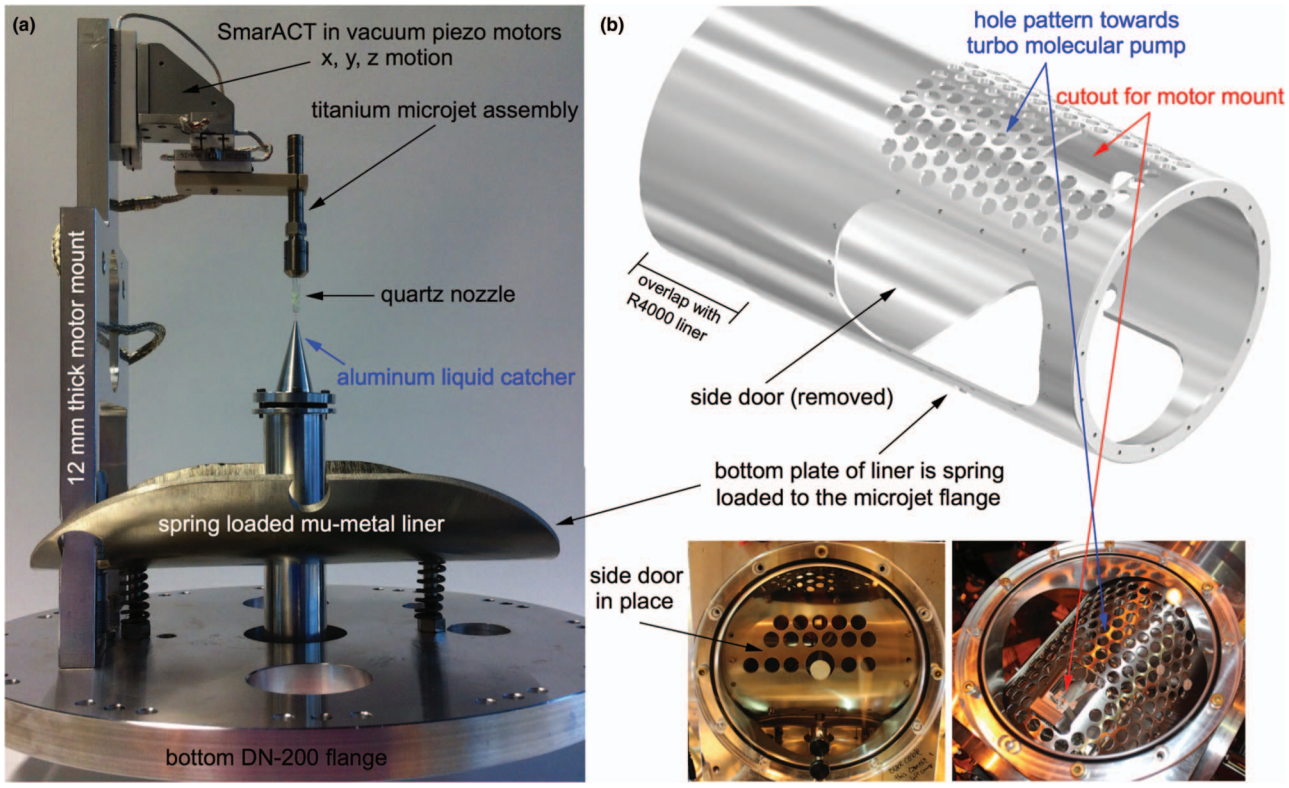

FIG. 2. (a) The liquid microjet and all of its components are mounted to the bottom DN-200 flange. (b) The mu-metal liner is designed to allow simple access to the measurement area. The overall magnetic field inside the liner with the liquid microjet installed is less than 15 μT.

electron spectrometer is equipped with a gold mesh installed in the pre-lens, traditional electrostatic lens modes designed for UV energies do not perform well on our system. At energies below ca. 60 eV, photoelectrons do not efficiently pass the gold mesh and the transmission function of the electron spectrometer becomes significantly reduced. To increase the low energy transmission function of our electron spectrometer we have developed an electrostatic lens mode that applies a positive potential to the L1p (L = lens, 1 = first element, p = pre-lens) element to accelerate low energy photoelectrons through the pre-lens system. The lens potentials of the accelerating 10 eV pass energy lens mode are shown in Figure 4 for photoelectron kinetic energies of 2–60 eV. We have also developed similar accelerating lens modes for pass energies of 20 and 50 eV. The accelerating potential increases linearly with increasing photoelectron kinetic energy. At low energies the accelerating potential needs to be reduced to prevent an unwanted large increase in the electron spectrometer

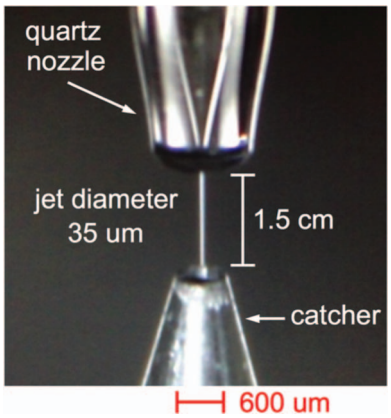

FIG. 3. The liquid microjet travels 1.5 cm inside the measurement chamber before it enters a 600 μm catcher and is directly drained outside the vacuum chamber where it can be recycled for further study. The diameter of the liquid microjet filament is variable, but typically in the 20–40 μm size range. The liquid filament depicted has been artificially enhanced for clarity.

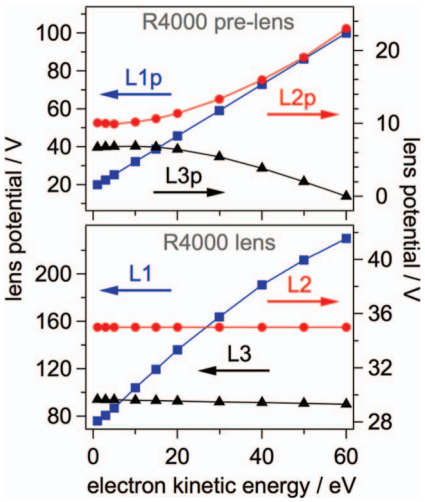

FIG. 4. Potentials applied to the six electrostatic lens elements of the Scienta *HiPP-2* R4000 electron spectrometer for 10 eV pass energy as a function of electron kinetic energy over the range of 2–60 eV. An accelerating potential is applied to the L1p element (see Figure 1(b)). At electron kinetic energies above 60 eV L1p is grounded and a traditional lens mode is employed.

transmission function (background electrons with energies on the order of several eV are accelerated into the lens).

C. Entrance cones

Applying a potential to the L1p element of the Scienta *HiPP-2* R4000 analyzer requires that we replace the traditional front entrance cone of the spectrometer with a truncated cone that exposes the L1p element to the measurement zone. Figure 5 shows both the truncated cone and the traditional ambient pressure cone. There are noticeable differences. The entrance aperture of the ambient pressure cone is between 0.1 and 0.8 mm and the cone-to-sample working distance is kept small, on the order of the aperture diameter. The truncated cone has an opening of 11 mm and a working distance of 9 mm. While together the truncated cone and accelerating lens mode allow for electron spectroscopy measurements from the liquid microjet at electron kinetic energies below 60 eV the design is not without its drawbacks. The 11 mm opening of the truncated cone no longer acts as a conducting restrictive aperture and introduces an upper pressure limit of 1×10^{-2} mbar in the measurement chamber. The large opening on the truncated cone also directly exposes the pre-lens to the liquid microjet environment. Long-term effects to the condition of the pre-lens with liquid microjet exposure remain to be evaluated. A major advantage of the truncated entrance cone is that the working distance is significantly increased. This proves beneficial when working with a liquid microjet to the point

FIG. 5. Entrance cones of the Scienta *HiPP-2* R4000 electron spectrometer used with the liquid microjet. The truncated cone exposes the L1p element to the measurement zone and allows for an accelerating field to be applied to photoelectrons below 60 eV. The working distance of the truncated cone is 9 mm. The traditional cone is used in liquid microjet studies at ambient pressure conditions up to 20 mbar and has an aperture diameter typically between 0.1 and 0.8 mm. The working distance of the traditional cone is on the order of the aperture diameter.

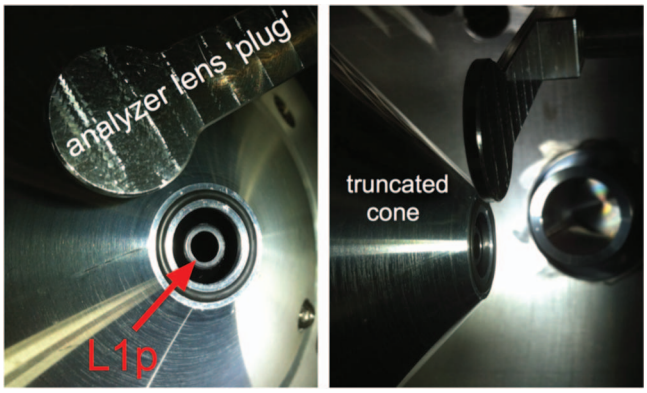

FIG. 6. A plug is used to seal off the electron analyzer vacuum system from the liquid microjet ionization chamber during venting and allows for quick venting of only the liquid microjet chamber. This manner of sealing off the analyzer works well and can maintain a vacuum of 1×10^{-8} mbar at the detector with the main analysis chamber vented to ambient air.

where the truncated entrance cone is now also used for XPS measurements where traditional lens tables are employed.

To avoid having to turn off the vacuum system and vent the analyzer each time the main analysis chamber is opened, i.e., to replace a clogged liquid microjet nozzle, we have designed a special "plug" that can be positioned in front of and pressed onto the truncated cone. Figure 6 shows this "plug" that consists of a small aluminum plate that is mounted to a linear/rotation feed-through. This manner of sealing off the analyzer works well and can maintain a vacuum of 1×10^{-8} mbar at the detector with the main analysis chamber vented to ambient air. When using the traditional entrance cone the differential pumping in the pre-lens is sufficient so that the analysis chamber can be vented to ambient air, while vacuum (10^{-6} mbar) is maintained in the hemisphere.

III. VACUUM SYSTEM

Opening up the energy analyzer to the liquid microjet chamber by using the truncated entrance cone described in Sec. II C introduces a significant water vapor load into the pre-lens section. Figure 7 shows a schematic representation of the vacuum system and the typical pressures in the various sections of the analyzer when the liquid microjet is in operation. The vacuum system is divided into five sections: the liquid microjet chamber (ionization chamber), the first and second differential pumping sections of the pre-lens, the lens, and the hemisphere. The ionization chamber is pumped with a 700 liter/s Agilent TwisTorr turbo molecular pump that is backed by an Agilent TriScroll 300 liter/min rough pump. Two Pfeiffer HiPace 300 liter/s turbo molecular pumps, each of which is backed by an Adixen 600 liter/min roots pump, evacuate the first differential pumping section of the pre-lens. Two Pfeiffer HiPace 300 liter/s turbo molecular pumps are also used to evacuate the second differential pumping section. The lens and hemisphere section of the analyzer are each pumped by a single Pfeiffer HiPace 300 liter/s turbo molecular pump. The turbo molecular pumps of the second differential stage, the lens, and the hemisphere are backed by a single Adixen 600 liter/min roots pump.

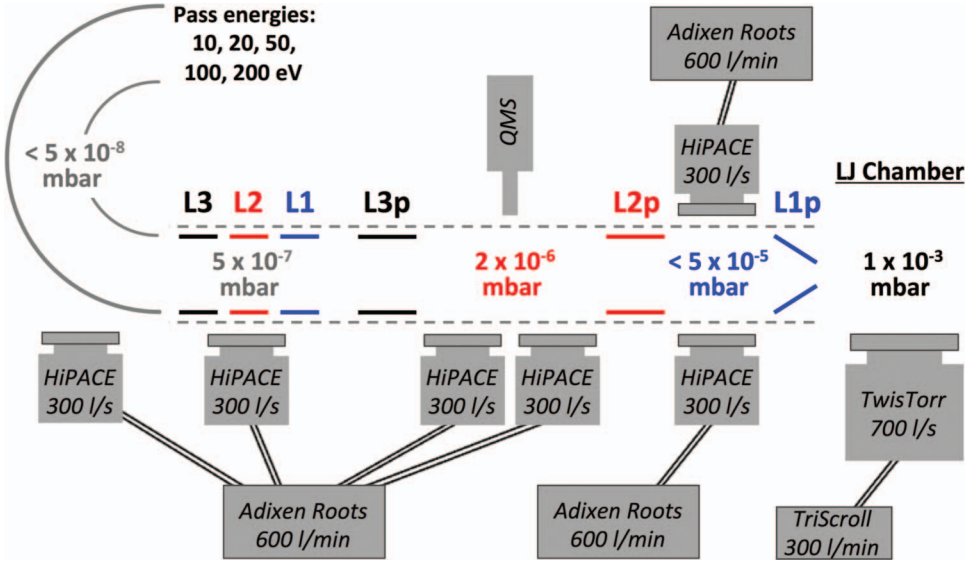

FIG. 7. A schematic representation of the vacuum system of the Scienta *HiPP-2* R4000 energy analyzer and the liquid microjet chamber. The pressures shown were recorded during operation of the liquid microjet with the truncated entrance cone.

The increased load brought about by using the truncated entrance cone affects predominantly the pre-lens vacuum with the lens and hemisphere sections experiencing little pressure change between liquid microjet operating conditions and when the ionization chamber is under moderate 1×10^{-6} mbar vacuum, i.e., when the liquid microjet is removed. The upper pressure limit for prolonged liquid microjet operation is 1×10^{-2} mbar above which the load on the two turbo molecular pumps of the first differential pumping section is too high. For liquid microjet experiments at pressures above 1×10^{-2} mbar the traditional entrance cone with an aperture diameter below 500 μm must be used.

IV. MOTION CONTROL OF THE ANALYZER FOR ALIGNMENT TO A BEAMLINE

The Scienta *HiPP-2* R4000 energy analyzer is mounted to an adjustable frame that allows for movement in the horizontal (x, y) and vertical (z) directions. The analyzer can be rotated in the (x, y) plane around a virtual axis passing through the analyzer focus, and tilted in the z direction. Wheels can be lowered from the frame for easy transport to and from a beamline. Commercially available motors, rails, and encoders are used for all frame movements. Linear movements in x, y, and z directions have a range of $\pm$50 mm with a resolution of 10 μm and a step reproducibility of $\pm$10 μm. The tilt and rotation ranges are $\pm$50 mrad with a resolution of 0.01 mrad and a reproducibility of $\pm$0.02 mrad. A LabVIEW program offering a convenient graphical interface that allows recording frame positions controls all movements.

V. PROOF-OF-PRINCIPLE MEASUREMENTS

All experiments were performed using 28–35 μm liquid microjets operating at 279 K and at a flow rate of 0.55–0.65 ml/min. The base pressure of the measurement chamber was 1×10^{-3} mbar.

A. X-ray photoelectron spectroscopy

The XPS synchrotron-based experiments described here were performed at the soft X-ray SIM beamline[22] of the Swiss Light Source. The liquid microjet endstation was connected to the beamline using a series of differential pumping stages separated by small apertures that allowed for windowless (e.g., silicon nitride) operation. The first aperture, which is mounted to the endstation, was 2 mm in diameter. A Pfeiffer HiPace 300 liter/s turbo molecular pump was used to maintain the vacuum in this section of the beamline at ca. 10^{-5} mbar. A second set of two apertures, each 5 mm in diameter, were mounted on either side of a second Pfeiffer HiPace 300 liter/s turbo molecular pump that maintained a pressure in this section of the beamline at ca. 10^{-7} mbar during liquid microjet operation. The remaining section of the beamline before the refocusing mirror, which generates a 60 μm horizontal spot size in the measurement chamber with the 50 μm vertical size set by the exit slit, was evacuated by two ion pumps, Agilent VacIon Plus 20, and Varian VacIon Plus 75. The pressure measured at the refocusing mirror chamber was 1×10^{-8} mbar during liquid microjet operation. As a precaution to guard against an unlikely pressure burst in the beamline from the liquid microjet, a fast closing VAT gate valve has been installed upstream of the refocusing mirror to protect the ultrahigh vacuum in the photoemission electron microscopy (PEEM) endstation of the beamline.[23] The pressure gauge with which the fast gate valve is interlocked is located behind the differential pumping section. The fast gate valve has a closing time of 10 ms after a detected pressure increase above 1×10^{-5} mbar.

A solution of 0.25 M butylamine was prepared by diluting a stock 99.5% solution (Sigma-Aldrich). The pH was adjusted to 10.2 by the addition of concentrated

37% HCl (Sigma-Aldrich) and measured using a Mettler Toledo Expert Pro electrode. The pH was chosen in such a way that the solution contained a mixture of both neutral butylamine and protonated butylamine according to the equilibrium, $CH_3CH_2CH_2CH_2–NH_2 + H_3O^+ \Leftrightarrow CH_3CH_2CH_2CH_2–NH_3^+ + H_2O$. The room temperature pKa of butylamine is 10.6.[24] Nitrogen 1s spectra were recorded as a function of photoelectron kinetic energy over the range 15–1000 eV. Spectra were fit using Gaussian functions following a standard background subtraction. At electron kinetic energies ≤60 eV the accelerating lens mode described in Sec. II B was used with pass energy 20 eV. At energies >60 eV, a 100 eV pass energy (traditional) lens mode was used that does not apply a potential to the L1p element. All spectra were recorded in vacuum (1×10^{-3} mbar) using the truncated entrance cone described in Sec. II C.

Nitrogen 1s photoelectron spectra collected from a 0.25 M solution of butylamine at electron kinetic energies of 35 and 995 eV are shown in Figures 8(a) and 8(b), respectively. These spectra are representative of the signal-to-noise ratio obtained throughout the energy range of 15–1000 eV studied herein. There are two well-resolved peaks in each spectrum that have been fit using Gaussian functions. As labeled in Figure 8, the two components are assigned as protonated butylamine (fit shown in red) on the low energy side and neutral butylamine (fit shown in blue) on the high-energy side. The assignment of the two components is confirmed by measuring solutions at low and high pH that contain only protonated and neutral butylamine, respectively (not shown). The relative signal intensity of the two components varies as a function of electron kinetic energy and is summarized in Figure 9. There is a distinct minimum in the $R–NH_3^+$: $R–NH_2$ ratio in the energy range 60–100 eV with the ratio increasing on both the low and high energy sides. The overall shape to the data of Figure 9 closely resembles the universal inelastic mean free path curve of solids,[25] but predicts the minimum in dilute butylamine aqueous solutions to be 50–100 eV lower than was reported by Ottosson for neat water.[26]

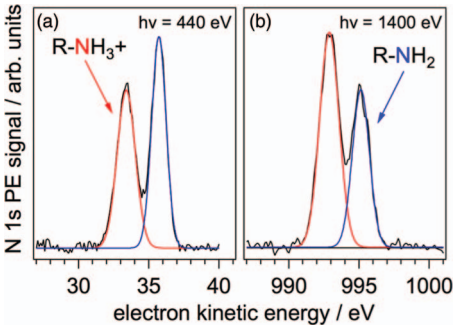

FIG. 8. Nitrogen 1s photoelectron spectra collected at (a) 35 eV and (b) 995 eV electron kinetic energy from a 0.25 M aqueous solution of butylamine. (a) Collected using the accelerating lens table presented in Sec. II B and shown in Figure 4. (b) Collected using a traditional lens table that grounds the L1p element. Both spectra were recorded using the truncated entrance cone. Each spectrum is fit using two Gaussian functions following standard background subtraction. The component at low kinetic energy is assigned to protonated butylamine (shown in red) whereas the component at high kinetic energy arises from neutral butylamine (shown in blue).

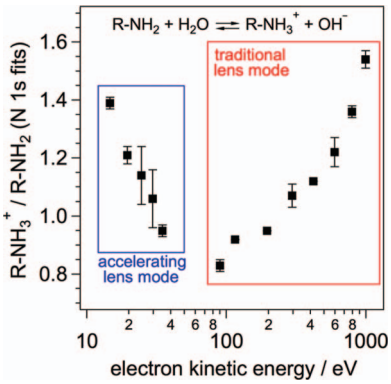

FIG. 9. The ratio of the integrated area of the $R-NH_3^+$ to $R-NH_2$ components of the nitrogen 1s photoelectron spectra from a 0.25 M aqueous solution of butylamine at pH 10.2 as a function of electron kinetic energy. The curve parallels the shape of the universal inelastic mean free path curve of solids.[25] A distinct minimum is evident between 60 and 100 eV. This energy window affords the most sensitivity to the vapor-water interface. At energies on both sides of the minimum the probe depth of the experiment increases.

The increasing $R–NH_3^+$: $R–NH_2$ ratio on the low energy side of the minimum suggests that the probe depth of the experiment is increasing with a decrease in photoelectron kinetic energy. Our results for the butylamine system demonstrate that the probe depth of the experiment at ca. 15 eV is equivalent to that when working at ca. 900 eV. In order to minimize the probe depth of photoelectron experiments from liquid solutions and in turn maximize (increase) the vapor-liquid interface sensitivity future experiments should be conducted in the 60–100 eV energy range. This 40 eV energy window should prove sufficiently large for future experiments to prevent photoelectron peaks, whose position depends linearly on incident photon energy, from overlapping with Auger peaks that do not change position with incident photon energy (when working on the kinetic energy scale).

B. Ultraviolet photoelectron spectroscopy

UPS experiments were performed using a commercial Scienta 5 K UV helium discharge lamp. The platinum coated torodial type monochromator (80 × 30 mm, 1200 lines/mm) was set to select the He II α line at 40.8 eV. Our experiments use a ca. 300 μm quartz capillary to focus the UV light onto the liquid microjet. The working distance is kept small, on the order of 2 mm. At this working distance the UV spot size is 350 μm. As discussed and shown below in Figure 10 the relatively large spot size compared with the diameter of the liquid microjet results in a significant contribution to the spectral intensity from the gas phase that makes spectral interpretation more cumbersome. Measurements were performed using a 0.05 M solution of NaCl with the truncated entrance cone.

Valence band photoemission spectra from a liquid microjet of 0.05 M NaCl are shown in Figure 10. The top spectrum, labeled "gas + liquid," is obtained when the liquid filament is in the optimal focal position in front of the energy analyzer and the UV source spot. The spectrum is a combination of both condensed water of the liquid microjet and gas phase water in the background volume of the chamber. The major contribution of the gas phase arises because the spot size of

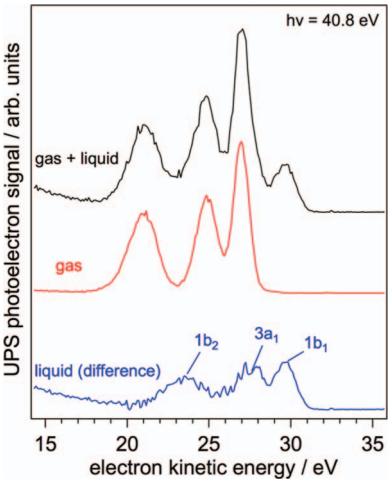

FIG. 10. Ultraviolet photoemission spectra recorded using He II α excitation at 40.8 eV from a liquid microjet of 0.05 M NaCl. The top spectrum is recorded with the liquid microjet in the focal plane of the electron analyzer and consists of both liquid and gas phase water. The gas phase spectrum is recorded by displacing the liquid microjet filament 500 μm away from the electron analyzer focus and out of the incident photon path. The difference spectrum provides the signature of liquid water.[13]

the UV source at 350 μm is much larger than that of the liquid microjet at 28 μm. The second spectrum in Figure 10, labeled "gas," is collected by displacing the liquid microjet filament 500 μm away from the focal plane of the energy analyzer and out of the UV source spot. In this manner only gas phase water is excited and the spectrum is noticeably different than that obtained for "gas + liquid." By taking the difference of these two spectra the valence band signature of pure liquid water is obtained. Assignments to the three orbital components in the spectrum labeled "liquid (difference)" are based on the work of Winter and co-workers.[13] We are at present designing smaller focusing capillaries that will reduce the UV spot size and in turn reduce the contribution from the gas phase.

C. X-ray absorption spectroscopy

The partial electron yield XAS synchrotron-based experiments described here were performed at the tender X-ray Phoenix beamline of the Swiss Light Source. The liquid microjet endstation was connected behind the permanent fluorescence endstation of the beamline using a straight vacuum section. No window (e.g., silicon nitride) was used during the experiments. Measurements were performed on a liquid microjet of a 10 wt.% colloidal Ludox CL silica nanoparticle suspension at photon energies of 1820, 1848, and 1876 eV, i.e., below, at, and above the Si K-edge, respectively, by integrating the Auger electron region of the spectra between 1500 and 1650 eV. Background measurements were collected for a liquid microjet of 0.05 M NaCl and the integral of the same region was used to establish an I_0 for normalization. The results of these three data points are compared to the full fluorescence yield XAS of a similar Ludox silica colloid[27] collected using the same liquid microjet when it was installed in the permanent fluorescence endstation of the Phoenix beamline at the Swiss Light Source.

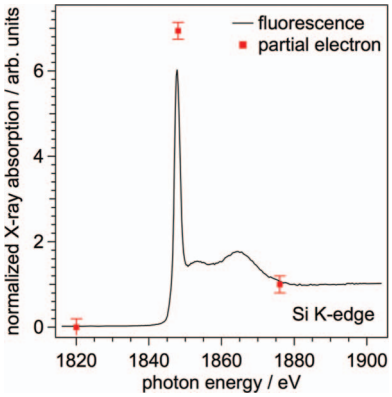

FIG. 11. (solid line) Normalized silicon fluorescence yield K-edge X-ray absorption spectrum from aqueous 3 wt.% colloidal SiO_2 Ludox SM collected with the liquid microjet installed in the permanent endstation of the Phoenix beamline.[24] (red squares) Partial electron yield XAS data collected using the new endstation from a liquid microjet of 10 wt.% Ludox CL at 1820, 1848, and 1876 eV.

Figure 11 shows the normalized fluorescence yield XAS for a 3 wt.% suspension of Ludox SM colloidal silica recorded using the liquid microjet when it was installed in the permanent endstation of the Phoenix beamline.[27] The three partial electron yield XAS data points recorded using the endstation presented herein are also shown in Figure 11 as red data points. The partial electron-yield data agree well with the fluorescence data and show a marked increase in absorption at 1848 eV.

Partial electron yield- and fluorescence-yield XAS measurements are complementary probes of the same physical process and each has certain advantages and disadvantages. Partial electron yield XAS probes the outer 1–10 nm of an interface due to the low inelastic mean free path of electrons in condensed matter,[25] whereas fluorescence yield XAS is generally considered a bulk probe. For example, the penetration depth of photons in water ranges from a few micrometers around 1 keV to about a millimeter at 7 keV.[28] The efficient detection of Auger electrons in partial electron yield XAS requires the background measurement chamber pressure to be below ca. 100 mbar, whereas fluorescence yield XAS can be performed at much higher pressures, simplifying certain *in situ* applications. In contrast to measurements in fluorescence mode, partial electron yield XAS does not suffer from self-absorption at high concentrations and allows for more concentrated solutes to be studied.

VI. CONCLUSION AND OUTLOOK

We have presented the new liquid microjet endstation that has been installed at the Swiss Light Source. First measurements at the soft X-ray SIM beamline (XPS), using a He II α source (UPS), and at the tender X-ray Phoenix beamline (XAS) were shown. Performing XPS measurements over a broad energy range from 1000 eV down to 15 eV allows for a depth resolved analysis of the solution composition near the vapor-water interface. The results obtained for a 0.25 M aqueous solution of butylamine at pH 10.2 indicate a distinct minimum in the probe depth of the experiment between 60 and

100 eV. At both lower and higher electron kinetic energies the probe depth of the experiment increases. UPS measurements neatly reproduce the shape of the valence band for liquid water by taking a difference spectrum from that of "gas + liquid" to "gas," the latter of which is recorded by offsetting the liquid microjet out of the UV source spot. At present, the relatively large spot size of our current UV source will prevent the trivial assignment of electronic structures with binding energies above the onset of liquid water. However, solutes with electronic structures below the onset of liquid water, such as halide ions,[5] will be easily distinguishable. Partial electron yield XAS measurements reproduce the Si K-edge absorption at the edge and post-edge regions that have been previously recorded using fluorescence detection.

Future developments involve interfacing the Scienta *HiPP-2* R4000 energy analyzer with the beamline control systems to allow for incident photon energy scans that will permit broad and continuous energy XAS measurements. Ambient pressure liquid microjet experiments that operate at the room temperature vapor pressure of the solution under study are also underway. These measurements use the traditional entrance cone and therefore do not allow for the use of the accelerating lens modes for low energy photoelectron detection. High-energy XPS experiments at the Phoenix beamline of the Swiss Light Source up to electron kinetic energies of 7000 eV are also in progress. High-energy measurements increase the probe depth of the experiment and allow for electronic structure measurements of bulk solutions.

One focus of this new endstation moving forward will be on studying electronic and geometric structures at the liquid-nanoparticle interface.[7] Scientific questions related to nanoparticle protonation state,[27] nanoparticle surface structure,[29,30] physical distribution of nanoparticles throughout the solution and their propensity for bulk solvation versus attachment to the vapor-liquid interface,[31] agglomeration, and dissolution of nanoparticles as a function of pH and in different electrolytes, and nanoparticle catalytic reactivity can be addressed. Our Scienta *HiPP-2* R4000 electron spectrometer will also be outfitted with a solid-state chamber, when the liquid microjet is removed, that will allow *in situ* electron spectroscopy measurements at the gas-solid interface under pressure conditions up to ca. 100 mbar. This chamber is currently being designed.

ACKNOWLEDGMENTS

Our near ambient pressure photoemission (NAPP) endstation is supported financially by PSI FoKo and the Swiss National Science Foundation R'Equip program (Grant No. 139139). We are indebted for the support of Friso van der Veen, Luc Patthey, Shunsuke Kato, Chris Milne, Markus Lampimäki, and Juraj Krempasky during the design, construction, and development phases. Finally, the whole Scienta team, but in particular Patrik Karlsson, Mårten Edwards, and Klas Backland, was instrumental throughout the design and commissioning stages of this project.

[1] H. Siegbahn and K. Seibahn, J. Electron Spectros. Relat. Phenom. **2**, 319 (1973).
[2] B. Winter and M. Faubel, Chem. Rev. **106**, 1176 (2006).
[3] P. Jungwirth and B. Winter, Annu. Rev. Phys. Chem. **59**, 343 (2008).
[4] M. A. Brown, M. Faubel, and B. Winter, Annu. Rep. Prog. Chem., Sect. C: Phys. Chem. **105**, 174 (2009).
[5] B. Winter, Nucl. Instrum. Methods Phys. Res. A **601**, 139 (2009).
[6] R. Seidel, S. Thürmer, and B. Winter, J. Phys. Chem. Lett. **2**, 633 (2011).
[7] M. A. Brown, I. Jordan, A. Beloqui Redondo, A. Kleibert, H. J. Wörner, and J. A. van Bokhoven, Surf. Sci. **610**, 1 (2013).
[8] See http://www.psi.ch/sls for specifications and operational performance of the Swiss Light Source.
[9] M. E. Grass, P. G. Karlsson, F. Aksoy, M. Lundqvist, B. Wannberg, B. S. Mun, Z. Hussain, and Z. Liu, Rev. Sci. Intrum. **81**, 053106 (2010).
[10] M. Faubel, B. Steiner, and J. P. Toennies, J. Chem. Phys. **106**, 9013 (1997).
[11] H. Siegbahn, L. Asplund, P. Kelfve, and K. Seigbahn, J. Electron Spectrosc. Relat. Phenom. **7**, 411 (1975).
[12] H. Siegbahn, S. Svensson, and M. Lundholm, J. Electron Spectrosc. Relat. Phenom. **24**, 205 (1981).
[13] B. Winter, R. Weber, W. Widdra, M. Dittmar, M. Faubel, and I. V. Hertel, J. Phys. Chem. A **108**, 2625 (2004).
[14] B. Winter, M. Faubel, I. V. Hertel, C. Pettenkofer, S. E. Bradforth, B. Jagoda-Cwiklik, and P. Jungwirth, J. Am. Chem. Soc. **128**, 3864 (2006).
[15] M. A. Brown, B. Winter, M. Faubel, and J. C. Hemminger, J. Am. Chem. Soc. **131**, 8354 (2009).
[16] M. A. Brown, F. Vila, M. Sterrer, S. Thürmer, B. Winter, M. Ammann, J. J. Rehr, and J. A. van Bokhoven, J. Phys. Chem. Lett. **3**, 1754 (2012).
[17] D. E. Starr, E. K. Wong, D. R. Worsnop, K. R. Wilson, and H. Bluhm, Phys. Chem. Chem. Phys. **10**, 3093 (2008).
[18] M. A. Brown, R. D'Auria, I.-F. W. Kuo, M. J. Krisch, D. E. Starr, H. Bluhm, D. J. Tobias, and J. C. Hemminger, Phys. Chem. Chem. Phys. **10**, 4778 (2008).
[19] M. J. Krisch, R. D'Auria, M. A. Brown, D. J. Tobias, J. C. Hemminger, M. Ammann, D. E. Starr, and H. Bluhm, J. Phys. Chem. C **111**, 13497 (2007).
[20] S. Ghosal, M. A. Brown, H. Bluhm, M. J. Krisch, M. Salmeron, P. Jungwirth, and J. C. Hemminger, J. Phys. Chem. A **112**, 12378 (2008).
[21] H. Bergersen, R. R. T. Marinho, W. Pokapanich, A. Lindblad, O. Björneholm, L. J. Saethre, and G. Ohrwall, J. Phys.: Condens. Matter **19**, 326101 (2007).
[22] U. Flechsig, F. Nolting, A. Fraile Rodriguez, J. Krempasky, C. Quitmann, T. Schmidt, S. Spielmann, and D. Zimoch, AIP Conf. Proc. **1234**, 319 (2010).
[23] L. Le Guyader, A. Kleibert, A. F. Rodriguez, S. El Moussaoui, A. Balan, M. Buzzi, J. Raabe, and F. Nolting, J. Electron Spectrosc. Relat. Phenom. **185**, 371 (2012).
[24] H. K. Hall, Jr., J. Am. Chem. Soc. **79**, 5441 (1957).
[25] C. J. Powell and A. Jablonski, J. Phys. Chem. Ref. Data **28**, 19 (1999).
[26] N. Ottosson, M. Faubel, S. E. Bradforth, P. Jungwirth, and B. Winter, J. Electron Spectrosc. Relat. Phenom. **177**, 60 (2010).
[27] M. A. Brown, T. Huthwelker, A. Beloqui Redondo, M. Janousch, M. Faubel, C. A. Arrell, M. Scarongella, M. Chergui, and J. A. van Bokhoven, J. Phys. Chem. Lett. **3**, 231 (2012).
[28] See http://henke.lbl.gov/optical_constants/ for Center for X-ray Optics, X-ray Database, Lawrence Berkeley National Laboratory (LBNL).
[29] M. A. Brown, R. Seidel, S. Thürmer, M. Faubel, J. C. Hemminger, J. A. van Bokhoven, B. Winter, and M. Sterrer, Phys. Chem. Chem. Phys. **13**, 12720 (2011).
[30] J. Söderstrom, N. Ottosson, W. Pokapanich, G. Öhrwall, and O. Björneholm, J. Electron Spectrosc. Relat. Phenom. **184**, 375 (2011).
[31] M. A. Brown, N. Duyckaerts, A. Beloqui Redondo, I. Jordan, F. Nolting, A. Kleibert, M. Ammann, H. J. Wörner, J. A. van Bokhoven, and Z. Abbas, Langmuir **29**, 5023 (2013).